Journal of Statistical Physics, Vol. 107, Nos. 1/2, April 2002 (© 2002)

Numerical Study of Axisymmetric Richtmyer–Meshkov Instability and Azimuthal Effect on Spherical Mixing

James Glimm,[1, 2] John Grove,[3] Yongmin Zhang,[1] and Srabasti Dutta[1]

Received March 8, 2001; accepted September 25, 2001

In this paper, we present a numerical study of the axisymmetric Richtmyer–Meshkov instability in converging spherical geometry by the front tracking method for the first time. The front tracking method has been successfully used in solving fluid instability problems in both rectangular and curved geometry.[1–6] The central issue for axisymmetric flows is the absence of the rotational symmetry in the (r, z) plane, although the perturbed shape of the initial contact interface appears to have it. The cause of the asymmetry is somewhat obvious. The sinusoidal perturbations appear symmetric only in the cross-sectional view; in actuality they are not symmetric because they represent rings around the z-axis and hence the perturbed mass at the equator, for example, is different from the perturbed mass at the pole. The first purpose of this paper is to quantify the effect of this inherited asymmetry on the growth of the spherical mixing. We find this asymmetry drives the original structure to some degree so that the mixing radius at the north pole is noticeably larger than at the equator during the evolution of chaotic mixing. We also study quantitatively the azimuthal dependence of the mixing statistics, such as the mixing edges, the growth rate and volume fraction. Richtmyer–Meshkov (RM) instabilities in spherical geometry have been a challenge due to the inherent difficulty of their accurate simulation. Our second purpose is to demonstrate that our Front Tracking method can describe the Richtmyer–Meshkov instability growth in a complex flow involving multiple reshocks. We have successfully displayed the converging geometry, reshock process, asymmetry phenomenon through the density and pressure color plots. The quantitative growth rate analysis is also presented.

KEY WORDS: Azimuthal asymmetry; axisymmetric instability; spherical mixing; Richtmyer–Meshkov; random interface.

[1] Department of Applied Mathematics and Statistics, University at Stony Brook, Stony Brook, New York 11794-3600; e-mail: yzhang@ams.sunysb.edu

[2] Center for Data Intensive Computing, Brookhaven National Laboratory, Upton, New York 11793-6000.

[3] Hydrodynamics Methods Group, Applied Physics Division, Los Alamos National Laboratory, Los Alamos, New Mexico 87545.

0022-4715/02/0400-0241/0 © 2002 Plenum Publishing Corporation

1. INTRODUCTION

In this paper we study quantitatively the physically based consequences of azimuthal asymmetry for a class of fluid instability and chaotic mixing problems of increasing interest. The chaotic mixing problems considered here are induced by a spherical shock wave crossing a perturbed spherical interface. (The shock induced instability is called a Richtmyer–Meshkov (RM) instability.) This geometry arises in studies of supernovae and in inertial confinement fusion (ICF). Full 3D simulations are difficult due to the requirements of grid resolution, more severe for the shock induced Richtmyer–Meshkov instabilities considered here than for the steady acceleration Rayleigh–Taylor instabilities. Most 3D multimode simulations of the latter have disagreed with experiment by factors of about two. For this reason, in the more difficult Richtmyer–Meshkov case, there will be a strong motive to try 2D simulations (for example spherical axisymmetrical ones). Pure mode spherical harmonic simulations are not significantly easier than spherical multimode simulations in most cases, since without special coding, at least one octant of the sphere (for even modes) must be simulated, in contrast to the planar case for which a single mode satisfies periodic boundary conditions which can readily be used to reduce the simulation size and thereby to allow sufficient numerical resolution for accurate simulations. For example the present simulations, if carried out for fully 3D spherical harmonic modes, would require an increase of computational resources by a factor of about 200. Similarly, the machining of fully 3D spherically harmonic perturbed spherical targets for laser driven experimental studies is more complex than it is for 2D axisymmetrically perturbed ones. Thus we expect that an effort will be made to extract as much information as is possible from the axisymmetric spherical instabilities. However, for axisymmetric flows, an important issue we have to consider is the absence of rotational symmetry. We should expect the lack of symmetry will introduce special structure into the instability and chaotic flow region it generates. The statistics of axisymmetric chaotic mixing should display dependence on both the radius r and the azimuthal angle ϕ.

The purpose of the present paper is to serve as a guide to and a limitation for any such program: Such studies are best confined to an equatorial region, and must be examined for the presence of axisymmetric bias. See Drake *et al.*[7] for an axisymmetric laser induced Richtmyer–Meshkov instability experiment and simulation, modeling late stage supernova ejecta dynamics. While the existence of the asymmetry can be predicted on theoretical grounds, its amplitude cannot, and thus we believe that the present study will be helpful in guiding future experiments and numerical simulations. In the context of ref. 7 the azimuthal asymmetry does not

appear to be serious. In the context of the present paper, we can explain this fact as due to the absence of reshock or very late time effects in ref. 7.

The central issues addressed in this paper, a quantitative assessment of azimuthal asymmetry and a study of the statistics of spherical mixing layers, has not been studied extensively, to the authors' knowledge. For the first time, we report here simulations results which are carried out successfully by our front tracking method for studying axisymmetric Richtmyer–Meshkov (RM) instabilities in both spherical and cylindrical geometries. We investigate the growth rate of a perturbation which is affected by: asymmetry, converging geometry and multiple reshocks. We study the dependence of the mixing statistics on the azimuthal angle in a detailed quantitative way.

The paper is organized as follows. In Section 2, by introducing the cylindrical coordinate system (r, z, θ), we exploit rotational symmetry and formulate the three-dimensional conservation law equations as two dimensional equations in r, z with additional source terms. We solve these equations in a domain $r \geqslant 0$. The numerical method is also described briefly. In Section 3, we present simulation results for the evolution of RM instability of an axisymmetrically perturbed sphere driven by an imploding spherical shock. The perturbation growth rate has been analyzed. The asymmetrical spikes near the north and south poles are observed during late time. In Section 4, we present simulations for RM instability in cylindrical geometry. The effect of the azimuthal asymmetry is studied. In Section 5, we study the effects of the asymmetry in the chaotic mixing resulting from random initial conditions. We also study the growth of the mixing layer and the volume fraction of the fluid penetration by taking both azimuthal (over a limited azimuthal range) and ensemble averages. We find the statistics near the north pole is different from the equator. The final section is reserved for conclusions and discussions.

2. EQUATIONS AND NUMERICAL METHOD

Axisymmetric flow is defined in terms of cylindrical coordinates (r, θ, z), where $x = r\cos\theta$, $y = r\sin\theta$, $z = z$. It is a flow independent of θ.

Let $\vec{e}_1 = (1, 0, 0)$, $\vec{e}_2 = (0, 1, 0)$, $\vec{e}_3 = (0, 0, 1)$ be the unit vector basis for the rectangular coordinate system. Let $(\vec{r}, \vec{\theta}, \vec{z})$ be the unit vector basis for the rotational coordinate system defined by $\vec{r} = \vec{e}_1\cos\theta + \vec{e}_2\sin\theta$, $\vec{\theta} = -\vec{e}_1\sin\theta + \vec{e}_2\cos\theta$, $\vec{z} = \vec{e}_3$. Let $\vec{v} = v_0\vec{r} + v_1\vec{z} + v_\theta\vec{\theta}$ be the fluid velocity, $\vec{g} = g_0\vec{r} + g_1\vec{z} + g_\theta\vec{\theta}$ be a body force, ρ be the mass density of the fluid, p be the pressure and $E = e + \frac{1}{2}\vec{v}\cdot\vec{v}$ be the total specific energy with the specific internal energy e. Under rotational symmetry, the Euler equations for a compressible inviscid gas are:

$$\rho_t + (\rho v_0)_r + (\rho v_1)_z = -\frac{1}{r}\rho v_0 \tag{1}$$

$$(\rho v_0)_t + (\rho v_0^2)_r + (\rho v_0 v_1)_z + p_r = -\frac{1}{r}\rho v_0^2 + \rho g_0 \tag{2}$$

$$(\rho v_1)_t + (\rho v_1 v_0)_r + (\rho v_1^2)_z + p_z = -\frac{1}{r}\rho v_1 v_0 + \rho g_1 \tag{3}$$

$$(\rho E)_t + (\rho E v_0)_r + (\rho E v_1)_z + (p v_0)_r + (p v_1)_z = -\frac{1}{r}\rho E v_0 - \frac{1}{r} p v_0 + \rho(g_0 v_0 + g_1 v_1) \tag{4}$$

The numerical method we use for computing RM simulations is a front tracking method, which is an adaptive computational method in which a lower dimensional moving grid is fit to and follows the dynamical evolution of distinguished waves in a fluid flow. In this paper, the evolution of a material interface (contact front) separating fluids of distinct densities is tracked. A detailed presentation of the axisymmetric algorithm for front tracking is given in ref. 3 together with a validation study. The ideas of front tracking can be described briefly as follows. We project the front dynamics into normal and tangential directions, which are thus split into two one-dimensional problems. The problem in the normal direction is an idealized jump discontinuity with local (smooth) variation on each side, i.e., a non-local Riemann problem. After updating the states on each side of the discontinuity, we move the front point by the computed wave speed. We then solve the problem in the tangential direction. Since this is a smooth problem, we use the Lax–Wendroff or MUSCL schemes to update the states along each side of the front. Finally we update the states in the interior smooth region using the Lax–Wendroff or MUSCL algorithms with the front data as a boundary condition. By tracking discontinuous waves one can include explicitly jumps in the variables across the waves and keep all discontinuities perfectly sharp. Thus we never perform finite differencing across the front. Therefore the main advantage of the Front Tracking method is that it completely eliminates the interfacial numerical diffusion that is inherent in any standard finite-difference method. This statement applies to mass diffusion as well as to interfacial vorticity, which is a leading contribution to numerical dissipation. In addition, the nonlinear instability and post-shock oscillations common to other methods are reduced by explicitly tracking the front. This method has been proved very successful in a wide range of interface instability simulations.[1,2,4–6] For a

more detailed description of the Front Tracking method, see Chern *et al.*[1] and Glimm *et al.*[2]

3. SPHERICAL RICHTMYER–MESHKOV INSTABILITY

In recent years, extensive research in RM instability has occured in modeling, experiment and simulation. Much of this literature is focused on planar geometry.[5, 8–16] Recently advances have been made in curved geometry, for which we refer to Zhang and Graham,[17, 6] Muller *et al.*,[18] Mikaelian,[19] Haas and Sturtevant,[20] Kuhl,[21] Sod,[22] Tubbs *et al.*,[23] and Chrien *et al.*[24] Here we will study the RM instability of three dimensional axisymmetric flow in spherical geometry. The general features of an RM unstable interface in spherical geometry are the following. As a spherical incident shock travels in the radial direction and collides with the perturbed material interface, it bifurcates into a transmitted shock and reflected wave. This stage is known as the wave bifurcation stage or a shock-contact interaction stage. At the end of the bifurcation stage, both the transmitted shock and reflected wave detach from the material interface. One wave propagates toward the origin, and the other wave away. For an open geometry, this outgoing wave will not interact with the material interface again. Accelerated by the incident shock, the material interface becomes unstable and fingers grow to form bubbles of light fluid and spikes of heavy fluid. The wave which moves toward the origin generates a pressure singularity at the origin, and is then reflected outward. As this reflected wave propagates outward, it interacts with the material interface again, a process known as reshock. Wave bifurcation occurs again, and this cycle continues. Therefore the material interface is reshocked many times, though each time the shock strength is weaker. Our experiment will be carried out for the shock imploding case, in which the initial shock moves into the material interface toward the origin.

The (r, z) computational domain is $[0, r_1] \times [z_0, z_1]$, with $z_1 = -z_0 > 0$. The origin is denoted by $P_0 = (0, 0)$. Let ρ denote the distance from any point in the computational domain to P_0. The contact surface is located at the perturbed circle $\rho = \rho_0 + a_0 \cos(m\phi)$ with a_0 the initial amplitude, m the frequency, and ϕ the azimuthal angle from the r-axis to the ray joining P_0 to the point at the contact. In our experiment, the inner fluid is SF_6 and the outer fluid is air. We place the incident shock wave in the air at the circle $\rho = \rho_1 > \rho_0$, and moving toward to the origin. Due to the rotational symmetry about the z-axis, we are considering a spherically imploding problem. The initial configuration of the system contains three regions: the region behind the incident shock, the region between the incident shock and the perturbed fluid interface, and the region enclosed within the

perturbed interface. The states ahead of the shock are initialized by the prescription of the densities inside and outside of the contact surface, the pressure and the velocities of two fluids. The state behind the shock is determined by a prescription of the pressure behind the shock front or the Mach number or the speed of the shock. A reflecting boundary condition is used at the left side, i.e., the $r = 0$ axis. Flow-through boundary conditions are applied at the top, bottom and right boundaries of the domain so that outbound waves will exit the domain. The idea of a flow through boundary condition can be briefly described as follows. In order to update the boundary state, we imagine there exists a far field state which is defined by the extrapolation of the states near the boundary point. Then we solve the Riemann problem using the interior state near the boundary and the extrapolated far field state and retain only the incoming waves. A flow through boundary is thus time-dependent. It is equivalent to an open boundary and an infinitely large domain. All waves will propagate out of the domain and no boundary signal will be reflected back at least theoretically. The physical parameters for our simulations are: the Atwood number $A = 2/3$, the initial amplitude to wave length ratio $a_0/\lambda = 0.06$, the frequency $m = 6$ and the shock Mach number $M = 1.2$.

Because SF_6 has greater density than air, spikes are outward pointing fingers of heavy (SF_6) fluid and bubbles are inward pointing fingers of air. The main quantities of interests are the amplitude a and the growth rate v which are defined as:

$$a = \tfrac{1}{2}(\rho_{sp} - \rho_{bb}),$$
$$v = \tfrac{1}{2}(v_{sp} - v_{bb})$$

where ρ_{sp} and ρ_{bb} are the distances from the origin P_0 to the tips of the spike and the bubble respectively, while v_{sp} and v_{bb} are the spike and bubble tip velocities in the radial direction. The computational domain is $[0, 8] \times [-8, 8]$ with 300×600 grid cells. The perturbed interface is given by $\rho = 6 + 0.2\cos(6\phi)$. The imploding shock is located at the circle $\rho = 6.21$ with the Mach number $M = 1.2$. We assume SF_6 and air are polytropic gases satisfying the gamma law with γ being 1.0935 for SF_6 and 1.4 for air. The densities are 5.1 for SF_6 and 1 for air. The pressure and velocity ahead of shock are 0.496 and 0. We ran the simulation up to $T = 31$. The evolution of the front is shown in Figs. 1–3. The growth rate and amplitude are plotted in Fig. 4. From this figure we first note that at the initial time the amplitude is reduced and the growth rate becomes negative. This is because the interface is compressed by the higher pressure behind the shock as the shock moves into the interface. After the shock is transmitted through the interface, we see that the growth rate has accelerated sharply.

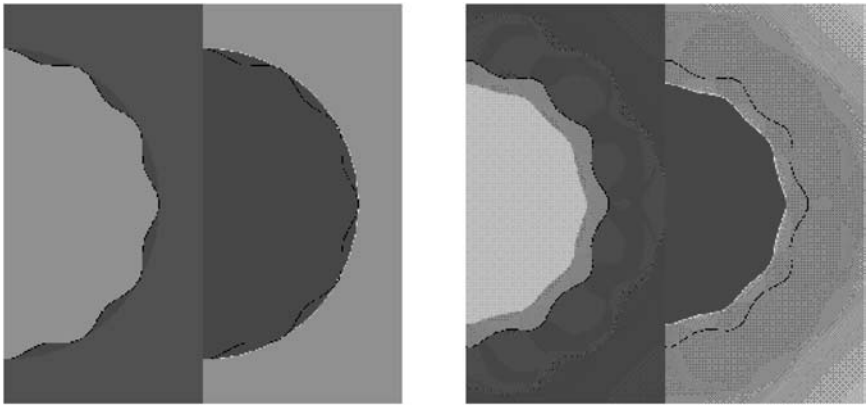

Fig. 1. A (r, z) cross-sectional view of the growth of instabilities in a spherical Richtmyer–Meshkov simulation for a 3D axisymmetric flow with a SF_6 spherical ball surrounded by air. In each pair, the left frame represents density and the right pressure. In the left pair, at $t = 0$, the spherical shock is moving radially toward origin and just about to hit the sinusoidal perturbed SF_6-air interface. In the right pair, at $t = 3$, both the inward transmitted shock and outward reflected wave are leaving the neighborhood of the interface and the perturbation has grown at an increased speed. The initial amplitude to wave length ratio a_0/λ is 0.06. The shock Mach number M is 1.2. The Atwood number A is $2/3$. The number of periods of sinusoidal wave perturbation in the full sphere is 12.

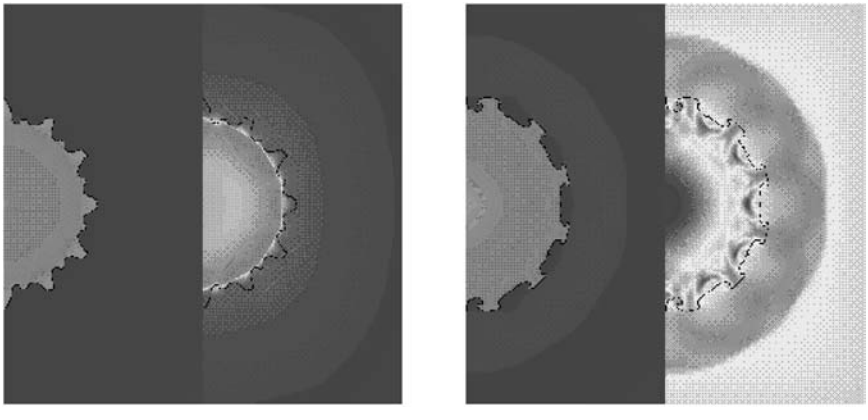

Fig. 2. In the left pair, at $t = 18$, the reflected shock is starting to hit the interface for the second time, an event called reshock. Phase inversion is taking place since the shock is transmitting the interface from a heavy fluid to a light one. In the right pair, at $t = 21$, the inversion has just completed and the growth rate has jumped from negative to positive. A very complicated wave structure is displayed in the pressure picture which shows that reshock is much more dynamic than the first shock.

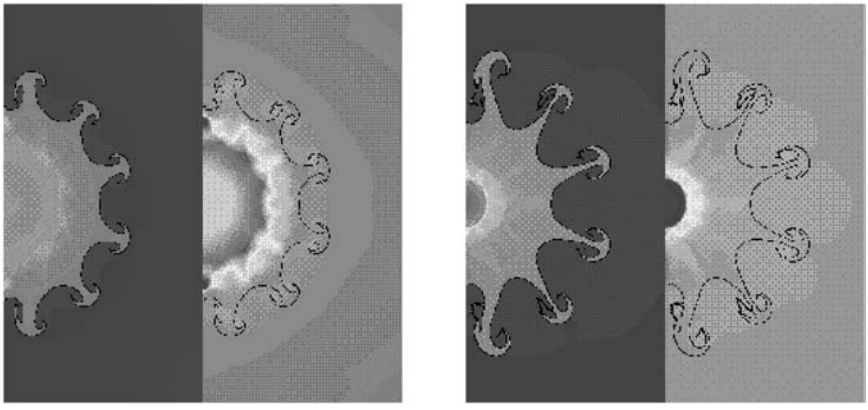

Fig. 3. In the left pair, at $t = 25.5$, the vortex rolling of the interface is observed. In the right pair, at $t = 31$, full bubbles and spikes have formed. The asymmetry is most noticeable at the spikes near the north and south poles.

From the front evolution plot (Fig. 2), we see that the shock hits the interface for a second time at $t = 18$, an event which is called reshock. From the growth rate plot (Fig. 4), we see the growth rate has a sharp drop at $t = 18$ due to phase inversion. When the incident shock implodes from light fluid to heavy as in the first passage of the shock, there is no phase inversion, whereas the phase inversion does occur when shock explodes

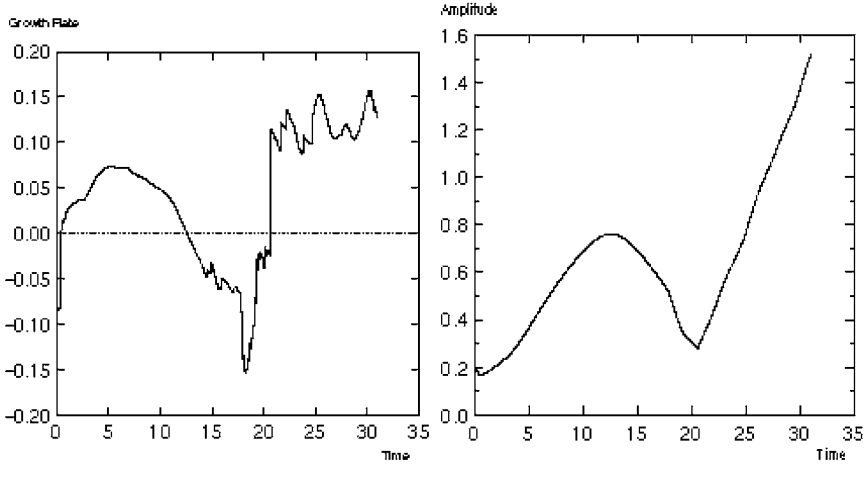

Fig. 4. Interface extrema data for a spherical Richtmyer–Meshkov simulation for a 3D axisymmetric flow with a shock of Mach number 1.2 imploding from air to SF_6 with an interface perturbed initially by 6 periods of a sinusoidal wave. Phase inversion takes place between $t = 18$ and $t = 21$. Left: growth rate. Right: amplitude.

from heavy to light at the time of reshock. In Fig. 4, there is a discontinuous jump in growth rate at $t = 21$ when the phase inversion is just completed and the original bubbles become the new spikes and the original spikes become the new bubbles. The phase inversion is also clearly demonstrated in the front picture (Fig. 2). From Fig. 3, we observe the formation of full bubbles and spikes at $t = 25.5$. We also observe asymmetrical spikes near the north and south poles. At $t = 31$, this asymmetry is most noticeable. The spikes at the north and south poles are leaning toward to the rotational axis. But the spikes lean toward the z-axis in a much weaker way at 45°. They show almost perfect symmetry near the equator.

4. CYLINDRICAL RICHTMYER–MESHKOV INSTABILITY

In this section, we conduct two experiments for a three dimensional axi-symmetric fluid in cylindrical geometry. The effect of asymmetry has been investigated in a detailed way.

In the first experiment, we place air on top of SF_6 in a rectangular domain $[0, r_1] \times [0, z_1]$ with the contact interface given by three periods of sine waves. The incident shock is generated in the air and moving downward into SF_6. Neumann boundary conditions are applied at the bottom of the computational domain so that the shock will reflect once it hits the lower boundary. Flow-through boundary conditions are imposed on the top of the domain, and reflecting boundary conditions are imposed on the left and right sides of the domain. The physical parameters are: the initial amplitude to wave length ratio $a_0/\lambda = 0.036$, the Mach number of the shock $M = 1.2$, and the Atwood number $A = 2/3$. We ran the simulation up to $T = 80$. The evolution of the front at times $t = 0, 13, 22, 38, 80$ is demonstrated in Fig. 5. At $t = 13, 22$, the asymmetry is not noticeable before reshock. After the reshock at $t = 38$, we start to observe an asymmetrical spike near $r = 0$ and the bubble position at the left boundary is slightly lower than the bubble at the right boundary. At $t = 80$, we observe the same phenomenon as in the spherical simulation, that is, the spike leans toward the rotational axis near $r_{\min}$ and the bubble grows faster at the left boundary than in other locations. We notice that this asymmetry is r-dependent, that is, the degree of the asymmetry is stronger as r is closer to $r_{\min} = 0$, which justifies the observation that in the spherical simulations strong asymmetry occurs in the north and south poles, weak asymmetry at the fingers at 45°, while we saw symmetric fingers near the equator due to the minimal variation of $1/r$.

It remains to be answered why the asymmetry is not noticeable before reshock. Is the asymmetry caused by reshock? In order to answer this question, we conduct the second experiment. We make the domain three

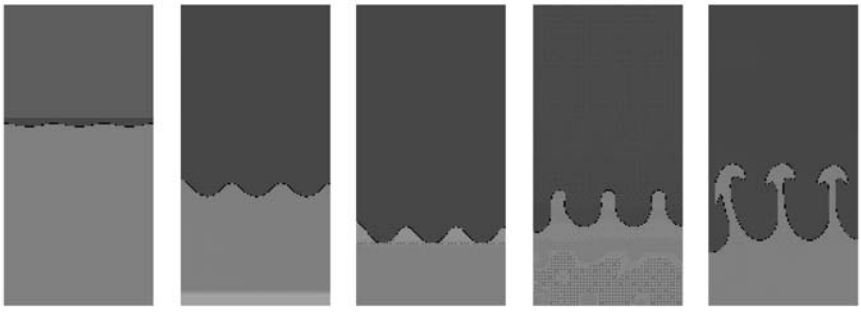

Fig. 5. The front evolution at times $t = 0, 13, 22, 38, 80$ in a cylindrical Richtmyer–Meshkov simulation for a 3D axisymmetric flow with light fluid (air) on the top of heavy fluid (SF_6). The initial perturbation and wave length ratio a_0/λ is 0.036. The shock Mach number M is 1.2. The Atwood number A is 2/3. The number of periods of sinusoidal wave perturbation $m = 3$. A Neumann boundary condition is located at the bottom of the domain. Initially at $t = 0$ the shock in the air travels downward toward the sinusoidally perturbed SF_6-air interface. At $t = 13$, the transmitted shock is about to hit the reflecting wall. Reshock is about to occur at $t = 22$. After the reshock, $t = 38, 80$, asymmetry of the spike near $r_{\min} = 0$ grows with time.

times as long in the z-direction as before so we can observe the growth of perturbation for a long time without a reshock effect. The initial amplitude to wave length ratio a_0/λ is set to be 0.24, which is about 6.6 times as large as in the first experiment, and comparable to the interface perturbation at the time of reshock, with other physical parameters unchanged. From the front evolution picture (Fig. 6), we see that the asymmetry increases with time. Therefore the asymmetry is not caused by reshock, but by the larger initial perturbation amplitude and the longer elapsed time of the simulation.

From these two experiments we can draw the following conclusions. First, the cause of the finger asymmetry is the variation of $1/r$, which is stronger as $r \to 0$. Therefore the degree of asymmetry is dependent on the r-coordinate. Secondly, the degree of asymmetry and time for it to occur also depend on the initial perturbation amplitude of the material interface. This explains why asymmetry is much stronger after reshock.

5. RANDOM INTERFACE

In this section, we study the asymmetry effect on spherical mixing during the evolution of the randomly perturbed spherical surface. We explore how the statistics of the spherical mixing, in particular, the volume fraction, the inner and outer edges, the growth rate of mixing layer, the radial and azimuthal velocities of the heavy fluid, will depend on the azimuthal location.

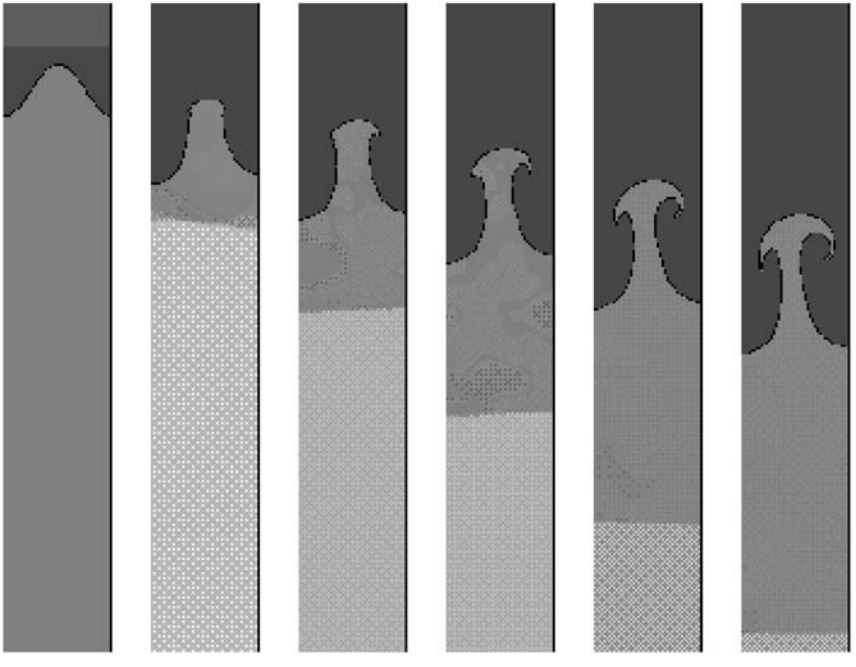

Fig. 6. Front evolution without reshock at times $t = 0, 16, 25, 36, 48, 60$ in a cylindrical Richtmyer–Meshkov simulation for a 3D axisymmetric flow with light fluid (air) on the top of heavy fluid (SF_6) with the interface perturbed by single period sinusoidal wave and the initial shock in air traveling downward toward the interface. The initial amplitude to wave length ratio a_0/λ is 0.24. The shock Mach number M is 1.2. The Atwood number A is 2/3. The bubble at the left boundary moves downward faster than the bubble at the right boundary. The asymmetry of the spike becomes stronger as time increases.

We conduct an imploding experiment with the spherical shock in air moving inward to the randomly perturbed axisymmetric SF_6 sphere. To save computational time, only a quarter domain is calculated. The nominally circular contact surface is given by superimposed Fourier mode perturbations in a finite frequency range with frequency expressed in units of the number of wavelengths n across a quarter arclength of the SF_6 surface, the respective minimum and maximum frequencies being $n_{\min} = 6$ and $n_{\max} = 12$. The average frequency is approximately the number of fingers that develop as the mixing enters a nonlinear stage. The initial interface profile $\rho(\phi)$ is given by the formula

$$\rho(\phi) = \rho_0 + \sum_{n=n_{\min}}^{n_{\max}} A_n \cos(4n\phi)$$

where the limits of the azimuthal angle ϕ are $\phi = 0$ and $\phi = \frac{\pi}{2}$, ρ_0 is about 70% of the width of the computational domain. The Fourier mode amplitudes A_n are generated by Gaussian sampling. The amplitude standard deviation is chosen to be about 0.02λ, where λ is the average wavelength of the perturbation.

We use flow-through boundary conditions at the top and right boundaries of the computational domain so that outbound waves will exit the domain. We impose the reflecting boundary conditions at the left and

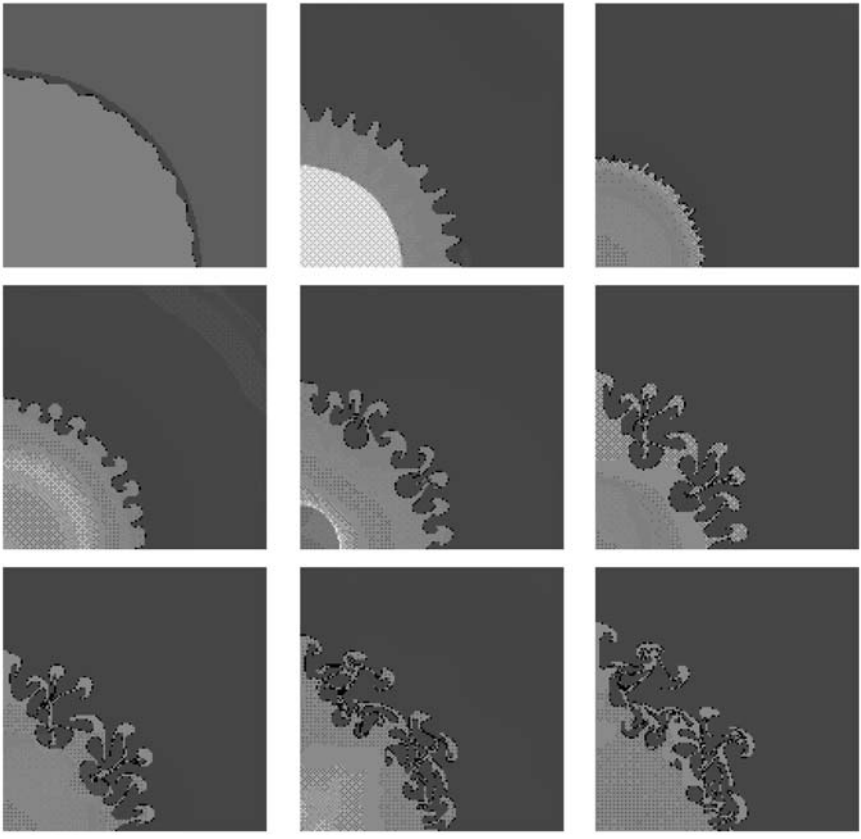

Fig. 7. Cross-sectional view of the growth of instability in a randomly perturbed axisymmetric SF_6 sphere driven by an imploding shock wave in the air. The top row shows the evolution at times $t = 0, 6, 17$. The third picture shows the first reshock, about to occur at $t = 17$. The second row shows the evolution at times $t = 24, 30, 38$. The third picture shows the second reshock, about to occur at $t = 38$. The third row displays the evolution at times $t = 40, 50, 60$. The shock Mach number M is 1.2 and the Atwood number A is $2/3$.

bottom boundaries due to the symmetry. The Atwood number $A = 2/3$ and the shock Mach number $M = 1.2$.

Figure 7 presents a sequence of frames for one realization of the statistical ensemble which shows the evolution of the instability and the late time chaotic mixing in the cross sectional plane. In particular, we use density plots to visualize the material interface and shocks, and the mixing process. Figure 7 depicts the evolution of the flow following a sequence similar to that described for the pure mode case. See also the caption to Fig. 7. We observe that the SF_6 surface becomes more aspherical at later times. We also notice that the mixing layer near the pole region has a bigger increase than the interface near the equator, and this trend becomes stronger as time increases.

In order to study how the asymmetry property affects the statistics of the axisymmetric chaotic mixing, we divide the computational domain equally into three fan-shape sectors by rays from the origin with azimuthal angles 30 and 60°. We refer the first sector to the equatorial sector, the second sector as the middle sector, the third sector to the polar sector. All the statistical quantities presented in this section are averaged over 20 realizations. Figure 8 presents the inner and outer edge radius, and growth rate of the mixing zone for each sector. We find the inner and outer edges have same radius among three sectors up to time $t = 18$ when the first reshock occurs. After reshock, the polar sector has a larger outer edge radius than the other sectors, and this difference grows as time increases.

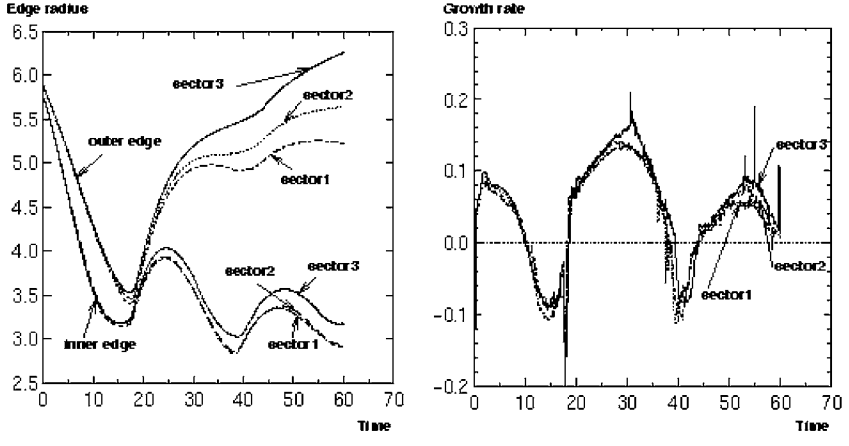

Fig. 8. The edges and growth rate of the sectorwise mixing layers for a 3D axisymmetric flow with a shock of Mach number 1.2 imploding from air to a randomly perturbed SF_6 sphere. Multiple reshocks take place at $t = 18$ and $t = 40$. The ensemble size $N = 20$. Left: inner and outer edges. Right: growth rate.

For the inner edge, the radius in polar sector is also larger than the other sectors, but the difference is relatively small and does not grow in time. It is also interesting to see that the difference between the equatorial sector and the middle sector only occurs in the outer radius, and is smaller than the difference between the polar sector and the others. The right picture of Fig. 8 shows that the polar sector also has larger mixing layer growth rate than the other sectors, and that the middle sector has larger growth rate than the equatorial sector to a smaller amount.

The most important quantity characterizing the mixing process is the mean concentration $\beta_k(t, x)$ of fluid k at spatial position x and t. In inertial confinement fusion, this function contains all of the information concerning the expected penetration of the instability. In astrophysics, β_k is a first order moment of the material interface geometry, an important ingredient for the statistical description of remnant formation.

Now we define an averaging procedure. We introduce the polar-coordinate system (R, ϕ) in the r, z plane by $r = R\cos\phi$, $z = R\sin\phi$, where $R = \sqrt{r^2+z^2}$, and ϕ is the azimuthal angle. We express flow field quantities in terms of these variables. The sectorwise azimuthal average of a flow quantity q in sector i is defined by

$$\langle q\rangle^i(R, t) = \frac{6}{\pi}\int_{\phi_i}^{\phi_i+\frac{\pi}{6}} q(R, \phi, t)\, d\phi \tag{5}$$

where $i = 1, 2, 3$, $\phi_i = 0, \frac{\pi}{6}, \frac{\pi}{3}$. The function X_k is the phase indicator for material k ($k = 1, 2$); i.e., $X_k(R, \phi, t)$ equals one if (R, ϕ) in fluid k at time t, zero otherwise. The sectorwise azimuthal average of X_k is the mean fluid k concentration or volume (layer, mixture) fraction in sector i, $\beta_k^i(R, t) \equiv \langle X_k\rangle^i$. Figure 9 presents the heavy fluid volume-fraction profiles β_2^i across the mixing layer within each sector at times $t = 30, 40, 50, 60$, averaged over $N = 20$ realizations. During the early times, we find little difference for β_2^i among all sectors and the difference is noticeable only starting around $t = 25$ when the reshock has occured. Figure 9 shows that β_2^3 is higher than β_2^1 and β_2^2 at later times, and this trend grows with the time. Therefore, for a fixed radius in the mixing layer, the heavy fluid concentration is much higher near the north pole than the other places. We also find the concentration in the middle sector is larger than the one near the equator, but it is significant only near the outer edge of the mixing layer. This characteristic of the heavy fluid concentration for each sector also explains why we observed earlier that the radius near the north pole is larger than the equator.

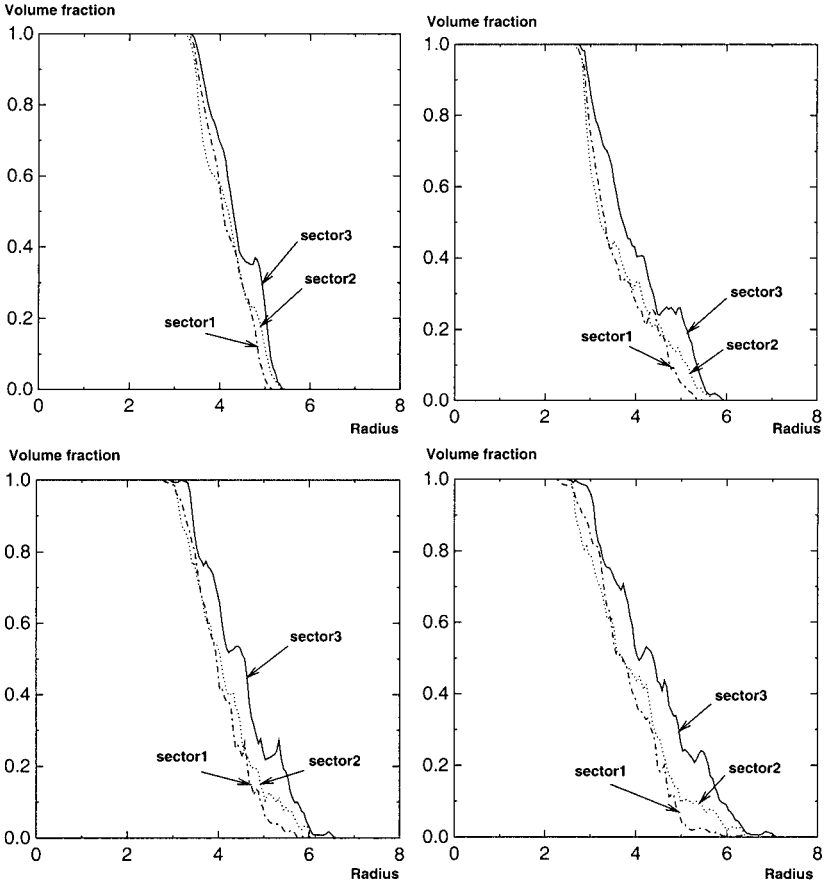

Fig. 9. Profiles of sectorwise heavy fluid volume fraction β_2^i at $t = 30, 40, 50, 60$, averaged over $N = 20$ realizations. The first row: $t = 30, 40$. The second row: $t = 50, 60$.

It is also interesting to study the sectorwise differences for radial and azimuthal velocities. We denote by $\bar{v}_r^i$ and $\bar{v}_\phi^i$ the sectorwise azimuthal average of the radial velocity v_r and the azimuthal velocity v_ϕ in sector i as defined in (5). We further take ensemble average average of $\bar{v}_r^i$ and $\bar{v}_\phi^i$ over the 20 realizations. Figures 10 and 11 present the profiles of the averaged radial and azimuthal velocities for $t = 30, 40, 50, 60$. We find a monotone increase of radial velocities from the equatorial sector to the polar sector near the outer edge of the mixing zone. This agrees with our earlier observation of monotone increase of the outer edge radius in Fig. 8. It is perhaps more interesting to note that azimuthal velocities are positive at all time for

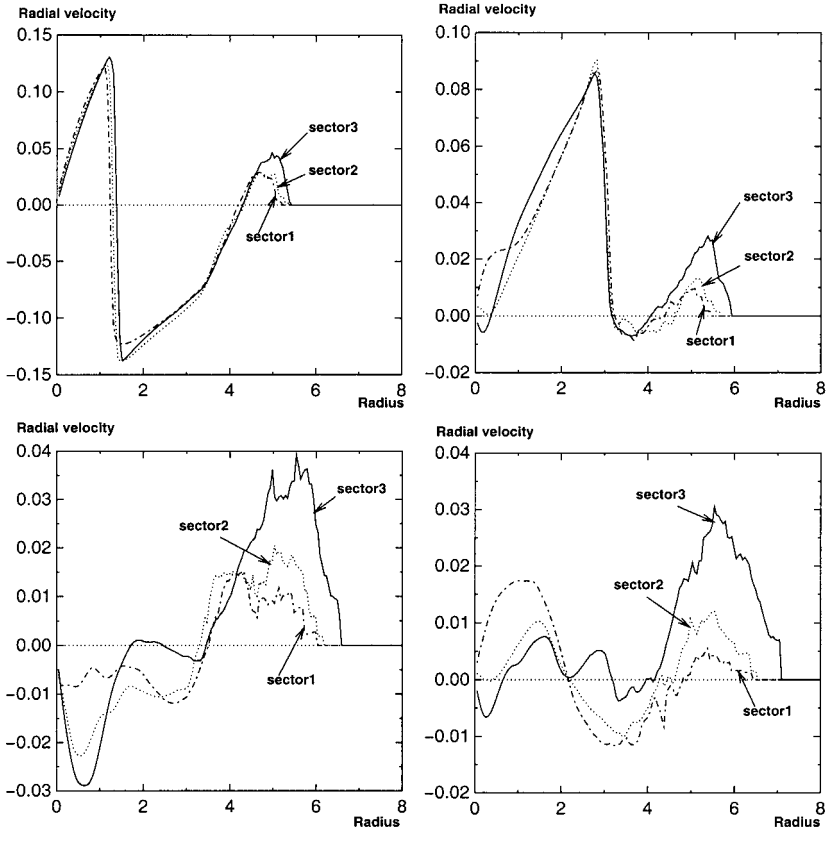

Fig. 10. Profiles of sectorwise heavy fluid radial velocities at $t = 30, 40, 50, 60$, averaged over $N = 20$ realizations. The first row: $t = 30, 40$. The second row: $t = 50, 60$.

each sector near the outer edge of the mixing zone, which indicates that the fluid near the outer edge moves toward the north pole region. In the three dimensional setting, the radius of the ring generated by rotating the z-axis becomes smaller as we move to the north pole. In the incompressible case, the larger cross-sectional area of fluid will be formed as the fluid moving toward the north pole, according to the mass conservation law. This explains why we saw the highest fluid concentration near the pole.

One question remained to answer is that why the sectorwise difference of statistical quantities is noticeable only at later time. During the early times, the azimuthal velocity is negligible compared to the magnitude of the radial velocity. Therefore the azimuthal movement is not visible, and thus we see little sectorwise difference in edge radius and volume fractions of

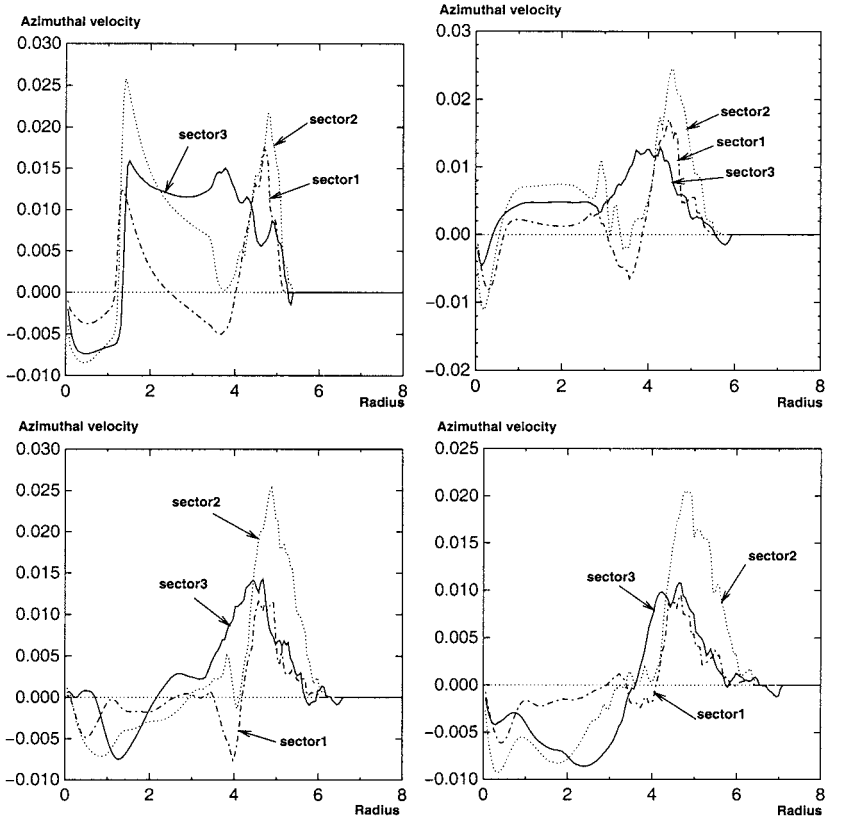

Fig. 11. Profiles of sectorwise heavy fluid azimuthal velocities at $t = 30, 40, 50, 60$, averaged over $N = 20$ realizations. The first row: $t = 30, 40$. The second row: $t = 50, 60$.

the mixing zone. After the multiple reshocks, the radial velocity becomes smaller and is comparable to the azimuthal velocity as the shock becomes much weaker. As more fluid moves into the north pole, the fluid is pushed upward and the radius there becomes bigger than the other places. Finally the original spherical surface evolves into a football shaped surface. Therefore a conclusion we can draw is that the asymmetrical statistics among the sectors is caused by azimuthal movement of fluid toward the north pole. At early time, this asymmetry is not noticeable due to the complete domination of the radial movement. At later time, the asymmetry is strongly present as the azimuthal motion increases while the radial movement is reduced with an increase in time.

6. CONCLUSIONS

In this paper, numerical simulations for axisymmetric RM instabilities in both spherical and cylindrical geometries have been successfully conducted by the front tracking method for the first time. The cylindrical coordinate (r, z) system used here has been shown suitable and effective in various axisymmetric fluid instability simulations. The cylindrical grid lines fit the rotational geometry better and significantly reduce the computing time by reducing the three dimensional conservation law equations to two dimensional ones which exploit the rational symmetry of the fluid. Our Front Tracking method has been proved to be effective in studying a variety of fluid-mechanic effects related to interface instabilities in spherical geometry. Our simulations have been carried out for both sine and random interfaces.

In the sine perturbed interface, we have studied a RM instability whose development is affected by (1) asymmetry; (2) converging geometry; (3) multiple reshocks. These three factors have been clearly demonstrated in both density and pressure color plots. The growth rate of the perturbation has also been analyzed quantitatively. We have studied the the effect of asymmetry in a detailed way. The degree of the asymmetry is related to the variance of $1/r$. The asymmetry is strongest near the pole since the biggest variation of $1/r$ occurs there. Therefore this asymmetry depends on the azimuthal angle ϕ. The degree of asymmetry and the time for it to occur also depends on the amplitude of the perturbation, which is why the asymmetry is not noticeable during early times.

For chaotic flows resulting from random initial conditions, the azimuthal angle ϕ introduces additional chaos to the spherical mixing process. We find this azimuthal dependence of mixing will introduce a deviation from a spherical structure as we observed that the radius of mixing near the pole region becomes noticeably larger than the radius at the equator during the chaotic mixing phase. We also find a higher volume fraction, and a larger growth of the mixing layer near the north pole than near the equator during the chaotic mixing phase. We have further demonstrated that the statistical difference between the north pole and the equator is caused by the azimuthal movement of the fluid toward the north pole.

Further analysis of the axisymmetric problem will be useful for ICF applications. In this context a number of questions can be studied by the present methods, such as a possible asymptotic description of the edges of the mixing zone, which behave as powers of t in the planar case. While we plan such studies in future work, we emphasize on the basis of the present paper that the studies should avoid the polar regions and should be examined for azimuthal bias.

ACKNOWLEDGMENTS

Glimm and Zhang were supported by the MICS Program of the U.S. Department of Energy under Grant DE-FG02-90ER25084, by the Department of Energy Office of Inertial Fusion, by the Army Research Office under Grants DAAG559810313 and DAAH049510414, by the National Science Foundation Grant DMS-9732876, by Los Alamos National Laboratories under contract number C738100182X. John Grove was supported by the U.S. Department of Energy.

REFERENCES

1. I.-L. Chern, J. Glimm, O. McBryan, B. Plohr, and S. Yaniv, Front tracking for gas dynamics, *J. Comput. Phys.* **62**:83–110 (1986).
2. J. Glimm, J. Grove, X. L. Li, W. Oh, and D. H. Sharp, A critical analysis of Rayleigh–Taylor growth rates, *J. Comp. Physics*, 169 (2001), Report No. SUNYSB-99-19, State University of New York at Stony Brook and LANL Report No. LA-UR-01-2300.
3. J. Glimm, J. Grove, and Y. Zhang, Interface tracking for axisymmetric flows, *SIAM J. SciComp* (2001), Submitted.
4. J. Glimm, O. McBryan, R. Menikoff, and D. Sharp, Front tracking applied to Rayleigh–Taylor instability, *SIAM J. Sci. Stat. Comp.* **7**:230–251 (1986).
5. J. W. Grove, Applications of front tracking to the simulation of shock refractions and unstable mixing, *J. Appl. Num. Math.* **14**:213–237 (1994).
6. Q. Zhang and M. J. Graham, A numerical study of Richtmyer–Meshkov instability driven by cylindrical shocks, *Phys. Fluids* **10**:974–992 (1998).
7. R. P. Drake, H. F. Robey, O. A. Hurricane, B. A . Remington, J. Knauer, J. Glimm, Y. Zhang, D. Arnett, D. D. Ryutov, J. O. Kane, K. S. Budil, and J. Grove, Experiments to produce a hydrodynamically unstable spherically diverging system of relevance, *Astrophysical Journal* (2000), LANL Report No. LA-UR-01-2301.
8. U. Alon, J. Hecht, D. Ofer, and D. Shvarts, Power laws and similarity of Rayleigh–Taylor and Richtmyer–Meshkov mixing fronts at all density ratios, *Phys. Rev. Lett.* **74**:534–538 (1995).
9. G. Dimonte, C. E. Frerking, and M. Schneider, Richtmyer–Meshkov instability in the turbulent regime, *Phys. Rev. Lett.* **74**(24):4855–4858 (1995).
10. E. E. Meshkov, Instability of a shock wave accelerated interface between two gases, *NASA Tech. Trans.* **F-13**:074 (1970).
11. M. Vetter and B. Sturtevant, Experiments on the Richtmyer–Meshkov instability of an air/SF_6 interface, *Shock Waves* **4**:247–252 (1995).
12. J. Grove, R. Holmes, D. H. Sharp, Y. Yang, and Q. Zhang, Quantitative theory of Richtmyer–Meshkov instability, *Phys. Rev. Lett.* **71**(21):3473–3476 (1993).
13. L. D. Cloutman and M. F. Wehner, Numerical simulation of Richtmyer–Meshkov instabilities, *Phys. Fluids A* **4**:1821–1830 (1992).
14. R. L. Holmes, B. Fryxell, M. Gittings, J. W. Grove, G. Dimonte, M. Schneider, D. H. Sharp, A. Velikovich, R. P. Weaver, and Q. Zhang, Richtmyer-meshkov instability growth: Experiment, simulation, and theory, *J. Fluid Mech.* **389**:55–79 (1999), LA-UR-97-2606.
15. A. L. Velikovich and G. Dimonte, Nonlinear perturbation theory of the incompressible richtmyer-meshkov instability, *Phys. Rev. Lett.* **76**:3112–3115 (1996).

16. D. L. Youngs, Numerical simulation of mixing by Rayleigh–Taylor and Richtmyer–Meshkov instabilities, *Laser and Particle Beams* **12**:725–750 (1994).
17. Q. Zhang and M. J. Graham, Scaling laws for unstable interfaces driven by strong shocks in cylindrical geometry, *Phys. Rev. Lett.* **79**:2674–2677 (1997).
18. E. Muller, B. Fryxell, and D. Arnett, Instability and clumping in SN 1987A, *Astron. Astrophys.* **251**:505–514 (1991).
19. K. Mikaelian, Rayleigh–Taylor instability and Richtmyer–Meshkov instabilities and mixing in stratified spherical shells, *Phys. Rev. A* **42**:3400–3420 (1990).
20. J.-F. Haas and B. Sturtevant, Interaction of weak shock waves with cylindrical and spherical gas inhomogeneities, *J. Fluid Mech.* **181**:41–76 (1987).
21. A. L. Kuhl, Spherical mixing layers in explosions, *Dynamics of Exothermicity: In Honor of Antoni Kazimierz Oppenheim*, J. R. Bowen, ed. (Gordon and Breach, 1996), pp. 291–323.
22. G. Sod, A numerical study of a converging cylindrical shock, *J. Fluid Mech.* **83**:785–794 (1977).
23. D. L. Tubbs, C. W. Barnes, J. B. Beck, N. M. Hoffman, J. A. Oertel, R. G. Watt, T. Boehly, D. Bradley, P. Jaanimagi, and J. Knauer, Cylindrical implosion experiments using laser direct drive, *Phys. Plasmas* **6**(5) (1999).
24. R. E. Chrien, N. M. Hoffman, J. D. Colvin, C. J. Keane, O. L. Landen, and B. A. Hammel, Fusion neutrons from the gas-pusher interface in deuterated-shell inertial confinement fusion implosions, *Phys. Plasmas* **5** (1998).